The Performance of HST as an Infrared Telescope

M. Robberto[a,c] A. Sivaramakrishnan[a], J. J. Bacinski[a], D. Calzetti[a],
J. E. Krist[a], J. W. MacKenty[a], J. Piquero[b] and M. Stiavelli[a,c]

[a]Space Telescope Science Institute,
3700 San Martin Drive, Baltimore, MD   21218   USA

[b]LMTO Thermal Systems,
7474 Greenway Center Drive, Suite 200, Greenbelt, MD   20770   USA

ABSTRACT

On the basis of the measured NICMOS performance in HST-Cycle 7 and Cycle 7N programs, we analyze the behavior of the HST optical assembly at IR wavelengths. An accurate analysis of the telescope thermal status allows us to estimate the backround flux observed by NICMOS, and compare it with the flux actually measured in different filters. The very close match between expected and measured fluxes confirms the validity of our model. A good understanding of the HST emissivity, which turns out to be lower than previous estimates, allows to predict with higher accuracy the performance of the future IR instruments on HST like NICMOS+cooling system and to specify critical design parameters for WFC3. Also, issues related to the long term stability of the system can be addressed more properly, providing useful quantitative insight on future missions such as the Next Generation Space Telescope.

Keywords: Infrared Astronomy, Hubble Space Telescope, NICMOS, WFC3

1. INTRODUCTION

At the time Hubble Space Telescope (HST) was launched in 1990, all five instruments mounted at the focal plane were able to get data in the ultraviolet regime down to wavelengths ≤ 1200Å, but only one (WF/PC) could observe in the visible at wavelengths longer than the R band. With the installation of NICMOS on Servicing Mission 2 (February 1997), the potential of HST was temporarily expanded into the infrared region up to 2.5μm. In the near future, Servicing Mission 3B (launch planned in June 2001) will revive NICMOS by providing a permanent cooling capability with the installation of a Closed Cycle Cooler. A few years later, Servicing Mission 4 will further enhance the IR performance of HST with the installation of WFC3, which will be equipped with a 1024×1024 HgCdTe detector with a $\sim 1.8\mu$m long wavelength cutoff. From then on, until the end of its planned lifetime (2010), the complement of HST instruments will be able to cover the near-infrared regime with a unique capability largely unforeseen at the time the telescope was designed.

Reasons for this extension of wavelength coverage are both scientific and technological. The near-IR is where the optical continuum of very distant objects is redshifted. At near-IR wavelengths one is also less sensitive to dust absorption which is commonly seen in visible wavelength observations of galaxies and star forming regions. A more detailed discussion of near-IR science in the context of WFC3 is presented by Cheng et al. (this conference). On the technical side, new detector and thermoelectric cooler technology allow for a much simpler instrument design with - in principle - unlimited lifetime and good radiation resistance.

The main objective of the Space Telescope Program was to put a 2.4 m telescope with excellent optical quality into orbit to obtain unmatched spatial resolution and ultraviolet sensitivity. A major effort was taken to address and control the effects that can affect the telescope Point Spread Function. In particular, the telescope pupil was accurately modeled,[1] taking into account effects like wavefront error, mirror surface irregularities, dust scattering and jitter. However, little attention was paid to the IR performance of the telescope, i.e. to the emissivity budget.

With the upcoming NICMOS refurbishement in Servicing Mission 3B (Cycle 10 Call for Proposal is in prepapration), and in the design phase of WFC3, we have re-evaluated the HST design from the point of view of its

infrared performance. This paper presents the results of this exercise. On the basis of pre-launch design studies and spacecraft telemetry, we have collected all the data needed to build a simple model for the telescope thermal emission (Section 2). In order to check the validity of our assumptions, we have extended the model to include the relevant parameters for NICMOS (Section 3). Then, using a computer code based on the most recent exposure time calculator for NICMOS, we have estimated the total background data measured by NICMOS at wavelengths longer than 2μm and compared it with the measured count rates (Section 4). We obtain a close match between the calculated and measured values. The results and a discussion of the residual uncertainties are presented in Section 5.

2. OVERVIEW OF THE HST CHARACTERISTICS

Early on during the design phase of HST, it was realized that in order to attain the ultimate optimal quality all the optical parts should be maintained in a thermal environment as stable as possible. Several studies addressed this issue, and considerable effort was put into thermal design and computer modelling. The designers eventually produced a system in which the thermal control is mostly passive, with extensive use of both insulation and surfaces with low absorption-to-emissivity ratios. To keep the temperature stable, a few critical components like the mirrors have thermostatically controlled heaters. Ten years of superb HST data confirm the value of this strategy. However, from the point of view of IR performance, the HST design is far from being "IR optimized".

In fact, HST is a warm telescope. The IR background flux collected by cooled focal plane IR instruments like NICMOS or WFC3 is dominated, at rather short wavelengths, by telescope thermal emission rather than by zodiacal scattering. NICMOS data show that the telescope background exceeds the zodiacal background at wavelengths longer than $\lambda \simeq 1.6\mu$m, the exact value depending on the pointing on the sky and on the position of the Earth on its orbit.[2]

The color temperature and intensity of the telescope thermal background depend upon the size, temperature and emissivity of the various opto-mechanical elements encountered by the optical beam, namely:

- the primary mirror (M1)

- the secondary mirror (M2)

- the central baffle inside M1

- the central baffle around M2

- the edge baffle surrounding M1

- the spiders

- the three pads on M1 holding the mirror.

Besides the mirrors, the most important factors in the emissivity budget of a telescope are the central hole in M1 and the oversized edges of M2. These regions should be efficiently masked by a well designed cold stop at the exit pupil, and this strategy in fact has been adopted by the HST IR instruments NICMOS and WFC3. However, as we shall see in Section 3, in the case of NICMOS a mechanical problem causes a significant pupil misalignement, and several parts of the entrance pupil (mostly baffles) supposed to be masked by the cold stop remain visible to the detector. For this reason we included a discussion of the thermal status of the telescope baffles in our analysis.

2.1. The primary mirror M1

The primary mirror of HST was fabricated in Corning ULE Titanium Silicate and coated with 650Å Aluminum and 250Å Magnesium Fluoride. The design temperature was 70 ± 2 °F, corresponding to 21.1 ± 0.5 °C. It is well-known that it was not built to spec, forcing HST instruments of the second generation and beyond to use extra optics to correct for the spherical aberration of the primary.

2.1.1. M1 temperature

The primary and secondary mirror temperatures play a very significant role in determining the intensity of the telescope thermal background. In particular, the design temperature of M1 was 70°F, but in fact the mirror is now operating at lower temperatures. In this section we summarize the current understanding of the thermal status of M1, on the basis of design studies and of the measured temperatures.

The primary mirror temperature is controlled by an array of 36 heaters located on the reaction plate behind the mirror. These heaters are maintained at 70 ± 1°F (21.1 ± 0.3°C). A Multi Layer Insulation (MLI) shell encases the reaction plate and M1, forming a radiation cavity that isolates the primary mirror/reaction plate from the Support System Module (SSM) aft temperature variations, and minimizes heater power. A temperature gradient is generated from the reaction plate to the back side and through the 12 inch thickness of the mirror, where the heat flow from the back to the front surfaces is two orders of magnitude greater than in radial directions. Numerical models show that within the mirror, which has a honeycomb structure, the temperature gradient is steeper in the core than in the front and back plates, since the conductance in the core is radiative and twice as effective as the material conductance in the plates.

Since the MLI conductively isolates the mirrors from the baffles, the front surface of M1 is closely radiatively coupled to the central and main baffle surfaces. A detailed knowledge of the baffle temperature and emissivity would be needed to investigate the degree of this coupling. Due to the fact that there is an high degree of symmetry in the baffle temperature distribution with respect to the telescope axis, the mirror temperature distribution is expected to be highly symmetric.

The front surface of M1 has six temperature sensors: three mounted at the outer edge and three at the inner edge within the central hole, at 120 degree angles. The measured temperatures are $\simeq 16$°C and $\simeq 14$°C, respectively, with variations less than 1°C, and no evidence for long term drifts on year-long time scales. On the mirror back (aft plate) there are 13 sensors which indicate that the back temperature is significantly warmer (roughly constant at 19 ± 0.5°C) than the front face.

Hereafter we assume an average temperature for the front face of the primary mirror of 15°C.

2.1.2. M1 emissivity

The HST primary (and secondary) mirror coatings have a measured emissivity of about 0.03. To this value we must add the contribution from the particulate material accumulated on the surface. Contaminations on the mirror reflecting surface are expected to increase the heat flow from the mirror, affect the radial temperature gradient and eventually will reduce the mirror temperature, unless the aft plate is heated more to compensate for the increased heat loss.

At launch, the HST contamination requirements met by the critical surfaces was 400B, where 400 refers to the particle distribution level and B to a maximum non-volatile residue (NVR, material remaining after evaporation of a liquid) level of 2mg/square feet, according to MIL-STD-1246. The fractional area covered by particles, or Obscuration Ratio (O.R.), can be estimated using the model of Ma, Fong and Lee[3] . These authors, using a wide spectrum of sphere/cylinder particle shape and size distribution, find a strong correlation between the MIL-STD-1246B cleanliness level and the obscuration ratio. In our case, O.R. $\simeq 0.1\%$. This value sets an upper limit to the emissivity. In principle, a dust particle that is large compared with the wavelength of light absorbs or scatters at wide angles the ligh falling on it, and diffractively scatters an equal amount. Therefore, a given amount of O.R. contributes about twice to the loss of throughput, but only once to the emissivity. Moreover, measurements done at Perkin-Elmer[4] on calcium carbide dust indicate emissivity about 50% of the O.R., due to a combination of thermal conductivity and intrinsic grain emissivity.

The HST was maintained in clean environment until launch. The launch vehicle itself had purge capabilities that continued until lift-off. Following lift-off, HST was exposed to the payload bay air venting. The cargo bay doors opened about one hour after lift-off. The most critical part was therefore the launch and ascent phase, due to possible contamination by material released during ascent. Increasing temperature and decreasing pressure during ascent may have caused spacecraft materials to outgas and deposit molecular contaminants on exposed surfaces.

Long term degradation in orbit is due to a combination of solar radiation damage and surface contamination. There is a gradual buildup of contaminants in orbit, possibly accompanied by a change in the optical properties of the contaminant, due to the radiation exposure. The source of contaminant is attributed to spacecraft outgassing

products and decomposition of materials exposed to radiation damage. The combined effect of these agents is difficult to estimate theoretically, therefore any measured loss of performance of HST may represent an important test case.

We do not expect any significant deterioration in the mirror coating. The NASA Long Duration Exposure Facility (LDEF) showed that the surface of a Quartz mirror sample coated with MgF_2 on Aluminum remained virtually unaffected by the 5.7 year long flight.

In conclusion, we assume as a baseline an O.R. $\simeq 0.1\%$ and the same value for the emissivity from the dust on the mirror. This turns out to be negligible in comparison to the 3% estimated for the Al coating.

2.2. The secondary mirror M2

The HST secondary mirror is made of Schott Zerodur and coated with Al and MgF_2 in the same way as M1. On the basis of the first order parameters of the HST optical design, the minimum size of M2 should be 266.90 mm to avoid vignetting on-axis sources. In fact M2 is 5% oversized, and its diameter of 281mm allows HST to produce an unvignetted circular field of ≈ 100 arcminutes. Therefore, for an on-axis beam, M2 sends to the focal plane the thermal emission from a ≈ 6.5 cm annulus encircling the primary mirror. Since the NICMOS cameras image a field off-axis by ≈ 7 arcmin, the geometry of the input pupil, and the corresponding distribution of thermal background, are sligthly asymmetric.

2.2.1. M2 temperature and emissivity

From the point of view of the thermal design M2 is a critical component, and a key concern has been to minimize its mean temperature change. The M2 assembly is controlled at 21.1°C±0.1°C by 12 heaters on the actuator mounting plates and on the shroud between the plates. The annulus between the actuator/shroud plates and the metering truss hub is insulated with MLI, as is the region between the shroud cover and the hub cover. All baffle surfaces facing into the secondary mirror housing cavity are covered with low-emittance tape or with MLI.

Six thermal sensors monitor the secondary mirror assembly, three on the back face and three at the edge close to the support structure. The mean temperatures read are 17°C and 18°C for each group, with dispersion less than 0.1°C. Pre-flight thermal analysis[5] and thermal vacuum test data show a gradient < 1°C between the coated mirror front face and back end. Hereafter we assume an average temperature of 17°C for the secondary mirror.

The same emissivity considerations developed for M1 also apply to M2. We shall therefore assume as a baseline an emissivity $\epsilon = 3\%$ for M2.

2.3. Baffles

Thermal control of the baffles is passive, and consists of minimizing the conductive coupling between the baffle mounts and the OTA structure so as to minimize heat leaks at these locations. Their temperature distribution is known from previous analyses as well as from temperature sensors placed on them. In particular, the Primary Mirror Thermal Analysis Report PR-442[6] describes the Central and Main baffle distributions for both hot and cold conditions, with results that are consistent with the measured temperatures.

The entire OTA is encircled by an outer "main" baffle, with temperature decreasing from the region around M1 to the outside. At the edges of M1, a ring protudes from the main baffle to create an "aperture" baffle encircling the mirror. Due to its high emissivity, the aperture baffle is at -14 ± 0.5°C, significantly colder than the mirror surface. The aperture baffle is the surface seen directly by the oversized M2 mirror outside the primary.

The two "central" baffles, one in the middle of M1 and the other around M2, are both equipped with only 2 thermal sensors on opposite sides with respect to the telescope axis. In the case of the M1 central baffle, the two sensors are located close to the primary mirror front face and show temperatures of ≈ 0°C. Thermal models indicate that there is a rapid drop-off in temperature in the aft fiberglass section of this central baffle, whereas in the forward (aluminum) part the drop-off is more gradual. Due to radiant interchange, the baffle temperature asymptotically approaches the main baffle temperature in the outward direction, dropping to values as low as -20°C to -40°C, depending on the environmental conditions of the telescope.

Measured M2 baffle temperatures are -19°C and -12°C, indicating that on the upper part of the telescope there are larger thermal gradients probably due to the anisotropy of the thermal load from the outer telescope parts. Like the aperture baffle for M1, a circular baffle surrounds the edges of M2 on the plane containing the mirror vertex. Large cold stop misalignment can cause light from this baffle to reach the instrument focal plane.
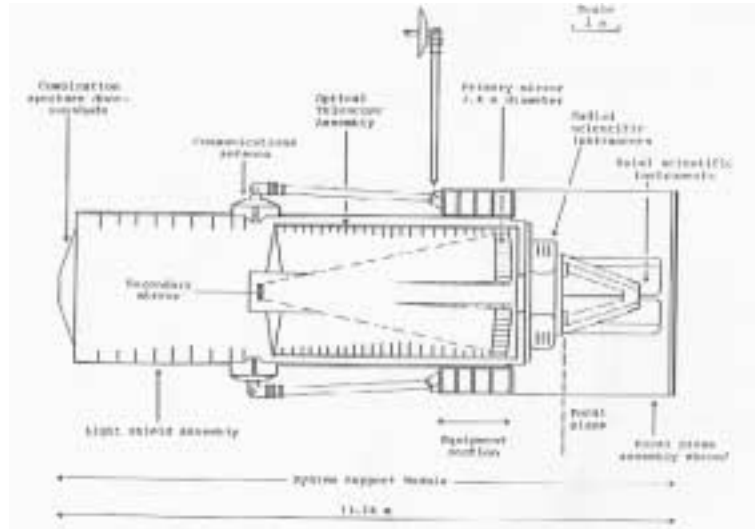
Figure 1. Schematics of the HST telescope.

We always assume emissivity $\epsilon = 1$ for the baffles, a condition virtually enforced by the low absorption-to-emissivity black painting.

2.4. Spiders

There are 7 temperature sensors on the 4 arm spider of the secondary mirror, placed half way on the arms. Three are on the mirror side and report an average temperature of $-15.5 \pm 1°$F, the others on the outer side with temperatures in the range $-18... - 21°$F. We assume emissivity $\epsilon = 1$ for the spiders.

2.5. Mirror pads

As shown in Figure 2, there are three circular areas on M1 that correspond to of the three pads holding the mirror to the aft plate. To minimize stray light in the optical bands, the outer surface of the forward mirror mount caps have been black painted and therefore have high emissivity. Like the primary mirror, they tend to be thermally coupled with the main baffle. To enforce the optimal thermal coupling with the front mirror surface, the thermal design used an $\epsilon \simeq 0.05$ coating on the inside of the mount caps, in order to have the same heat-loss/area at the mirror optical surface.

3. NICMOS

The actual IR performance of the HST can be estimated from the data provided by NICMOS (Near Infrared Camera and Multi-Object Spectrograph[7]). The thermal background seen by NICMOS has been analysed in several STScI Instrument Science Reports, mostly with the aim of addressing the background stability with respect to the position on the sky, i.e. before and after large slews, and long observation times. Background stability is crucial for sky subtraction and ultimate sensitivity. The data show that the HST thermal emission is fairly stable, with an orbital variation of $\sim 5\%$ and a secular variation of $\sim 8\%$, both in correlation with the temperature of the telescope optics.[8] This correlation enforces our hypothesis that a realistic model for the telescope background flux should be able to predict the measured background. In this respect, the earlier versions of the NICMOS Exposure Time Calculator are of little utility since their throughputs are fine tuned to match the observed fluxes.

With the exception of the dewar window, the filters and grisms, and the cold pupil stop, all the optical elements of NICMOS are reflecting surfaces located outside the dewar, i.e. at a temperature of $\approx 270°$C. The beam from M2 is reflected 7 times: 1 reflection on the pupil alignment mirror, 2 reflections for the correction of the conic error of M1, 1 reflection on the Field Divider Assembly that creates the three separate imaging fields. For each field there are 3 relay mirrors that re-image the telescope focal plane on three detectors with different magnifications.

Figure 2. The HST primary mirror at Perkin Elmers, with two of the three pads clearly visible in the mirror .
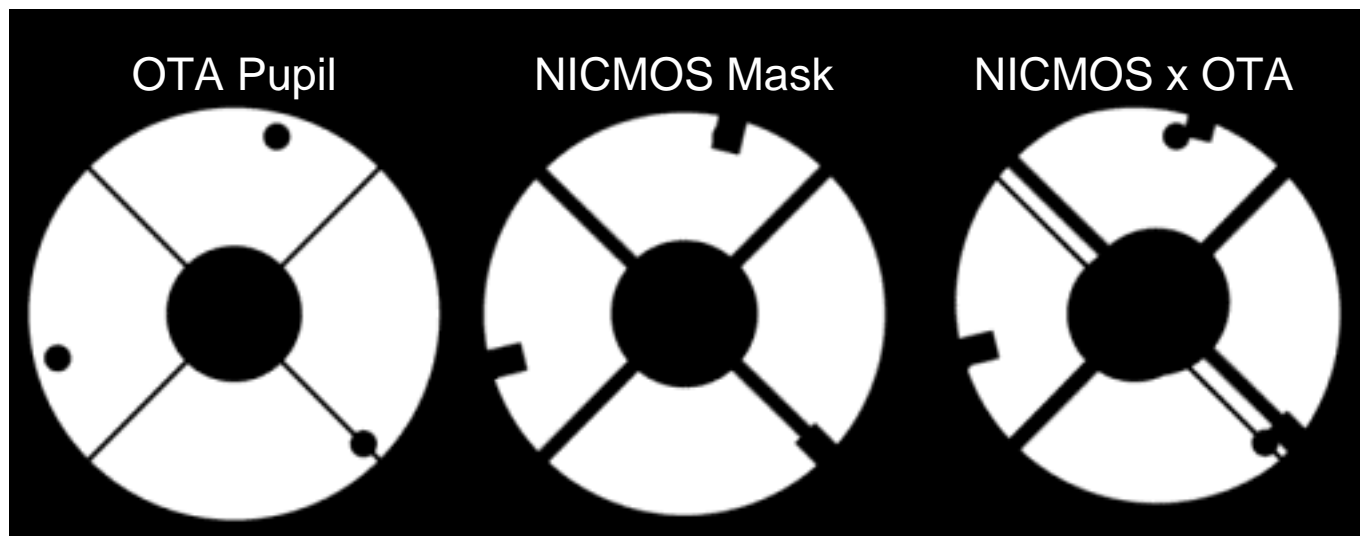

Figure 3. *Left:* The HST pupil, showing the secondary mirror support, spiders and mirror support pads. *Middle:* The NICMOS2 cold mask. *Right*: The HST pupil combined with the NICMOS cold mask shifted by 11% (From Krist et al., 1998).

A dewar anomaly related to the maintenance of the cryogenic conditions within the solid nitrogen vessel caused a deformation of the optical bench holding the detectors. As a result, the holding time of the cryogen was reduced from $\approx$ 5 years to less than 2 years, and complete depletion occurred in late December 1998. Moreover, the three detectors are no-longer confocal, with variations in plate scale, amount of aberrations, and – most important from the point of view of the IR performance – in the optical alignment of the instrument. In particular, the cold mask is no longer aligned with the telescope entrance pupil. A detailed analysis[9] of the NICMOS Camera 2 optics shows that the actual Point Spread Function, namely the shape of the diffraction rings and the banding pattern of the diffraction spikes, can be modeled by shifting the cold mask by about 11% of the pupil radius (Fig.3) Over time, the cold mask moves around the 11% mean value with an amplitude of 0.5%, which is negligible for our purposes.

Due to the optics misalignment, warm portions of the of exit pupil that were supposed to be masked by the cold stop become visible. In Table 1 we list the various surfaces seen by the NICMOS 2 detector and their filling factors within the solid angle seen by each pixel. The horizontal lines separate the three configurations shown in Figure 3, i.e. OTA pupil, NICMOS mask design and OTA+shifted mask.

Table 1. HST and NICMOS 2 pupil coverage (see text).

Surface	Area (cm^2)	Area (%)
total clear area	38990	0.86
high emissivity area	6250	0.14
total clear area	33415	0.74
masked area	11824	0.26
total clear area	30363	0.67
edge region not masked	1603	0.04
central region not masked	470	0.01
pads not masked	252	0.006
spiders not masked	236	0.005
cold mask projected onto M1	11080	0.24

The background fluxes measured by NICMOS 2[7] are presented in Table 2. We refer to three medium-band filters, F207M, F222M and F237M, as they provide higher background signals. Their central wavelengths are longer than 2μm, i.e. red enough that the zodiacal scattering contribution is negligible compared to the telescope thermal emission.

4. COMPUTER MODEL AND RESULTS

To model the background flux measured by NICMOS we used a new thermal library developed for the HST NICMOS camera for cycle 10 observations.[10] The library uses data files from STScI's Calibration Data Base System (CDBS) which describe the wavelength dependence of filter throughput and detector quantum efficiency for NICMOS' camera 2. The library is written in ANSI C and uses the CFITSIO library.[11] It is compiled with gcc and runs under Solaris and Linux operating systems.

The library treats the telescope and the camera as two objects in cascade. Starting with an etendue consistent with the entire entrance aperture (the area of the outer circle of the primary mirror), the new program implements a repeated application of Kirchoff's law to estimate the various contributions to the energy incident on a pixel. The various obstructions in the optical path are taken into account according to their emissivities, temperatures and pupil filling factors. Grey optics are assumed, i.e. emissivities and reflectivities are independent of wavelength.

The thermal contribution of each warm optic is calculated at 1000 points over the three NICMOS 2 filter bandpasses. A driver varying the primary and secondary mirror temperatures and emissivities for NICMOS' camera 2 was written in order to explore the primary and secondary mirror temperature parameter space and determine which combinations of emissivity, primary and secondary temperatures matched the observed backgrounds in these long wavelength filters.

5. RESULTS

5.1. OTA performances

The count rates estimated by our model, assuming the parameters described in the previous sections, are given in the last column of Table 2.

Table 2 shows that our results are in very good agreement with the observed values, which are overpredicted by a factor 6%, 6%, and 8% respectively, of the order of the temporal background variations. This indicates that the basic assumptions of our model are correct. If the measured data are representative of the average background, then to reach an almost perfect match it is necessary to reduce some dominant emissivity factor, such as the emissivity of the OTA mirrors or of the NICMOS camera. For example, reducing the emissivity of the OTA from 0.03 to 0.025 would

Table 2. Background count rates for selected filters in NICMOS 2

Filter	λ_c (μm)	$\Delta\lambda$ (μm)	Background (e/s/pix)	Model (e/s/pix)
F207M	2.08	0.15	2	2.11
F222M	2.22	0.14	7.8	8.27
F237M	2.37	0.15	31	33.4

provide an almost perfect match. Since we don't know the emissivity vs. scattering efficiencies for these surfaces at the wavelengths of interest, this exercise remains somewhat academic. Also, it seems difficult to be sure of how such small differences are distributed between the various HST/OTA and NICMOS surfaces.

Our slightly overestimated values provide a realistic, although conservative, basis for estimating the OTA emissivity, allowing us to address with more confidence the requirements on the amount of emissivity allowed for the science instruments, and on the cooling (i.e. dark current) of the IR detectors.

We note that the loss of throughput due to the pupil misalignement is over-compensated by the background arising from the high emissivity parts in the beam. We estimate for a hypothetically well-aligned NICMOS 2 camera a background flux 11% lower than the observed flux. Our estimates also resolve previous discrepancies in HST background calculations, which yielded results that were about twice the observed values at longer wavelengths. In particular, the emissivity of the OTA mirrors must be significantly smaller than the 5% value previously assumed in various studies. From the emissivity viewpoint, the HST mirrors appear have acquired no significant particulate contamination about 10 years after the launch.

6. CONCLUSIONS

We have considered the problem of the thermal emissivity for the HST telescope. We have built a model that correctly estimates the count rate in three NICMOS-2 filters starting from the current best knowledge of the telescope status. This work solves previous discrepancies in the estimates of emissivity of HST. A clear understanding of HST at IR wavelengths can have a significant impact on various factors, such as the definition of optimal cold optics temperature and of the cutoff wavelength for the H filter for WFC3, as one wants to avoid the long wavelengths where the OTA and warm instrument emission dominates the sky.

ACKNOWLEDGMENTS

REFERENCES

1. Burrows, C., 1990, HST Optical Telescope Handbook, version 1.0. (Baltimore: STScI)
2. Daou D. & Skinner, C., 1997, HST Instrument Science Report NICMOS-97-025. (Baltimore: STScI)
3. Ma, P. T., Fong, M. C., & Lee, A. L., 1989, SPIE 1165, 381.
4. Perkin-Elmer Optical Technology Division, OTA project Report 1282, 1987
5. Perkin-Elmer Optical Technology Division, OTA project Report 225, 1979
6. Perkin-Elmer Optical Technology Division, OTA project Report 442, 1980
7. MacKenty J.W. et al., 1997, NICMOS Instrument Handbook, Version 2.0, (Baltimore: STScI)
8. Daou, D., & Calzetti, D., 1998, HST Instrument Science Report NICMOS-98-010, (Baltimore: STScI)
9. Krist, J. E., Golimowsky, D. A., Schroeder, D. J., & Henry, T. J., 1998, PASP, 110, 1046.
10. Sivaramakrishnan, A., Holfeltz, S., Sosey, M. & Robberto, M., 2000, HST Instrument Science Report NICMOS-00-001 (Baltimore: STScI)
11. Pence, W., 2000, available on *http://heasarc.gsfc.nasa.gov/docs/software/fitsio/fitsio.html*